Facilitation dynamics and localization phenomena in Rydberg lattice gases with position disorder

Matteo Marcuzzi,[1,2] Jiří Minář,[1,2] Daniel Barredo,[3] Sylvain de Léséleuc,[3] Henning Labuhn,[3] Thierry Lahaye,[3] Antoine Browaeys,[3] Emanuele Levi,[1,2] and Igor Lesanovsky[1,2]

[1] *School of Physics and Astronomy, University of Nottingham, Nottingham, NG7 2RD, United Kingdom*
[2] *Centre for the Mathematics and Theoretical Physics of Quantum Non-equilibrium Systems, University of Nottingham, Nottingham, NG7 2RD, United Kingdom*
[3] *Laboratoire Charles Fabry, Institut d'Optique Graduate School, CNRS, Université Paris-Saclay, 91127 Palaiseau cedex, France*

We explore the dynamics of Rydberg excitations in an optical tweezer array under anti-blockade (or facilitation) conditions. Due to the finite temperature the atomic positions are randomly spread, an effect that leads to quenched correlated disorder in the interatomic interaction strengths. This drastically affects the facilitation dynamics as we demonstrate experimentally on the elementary example of two atoms. To shed light on the role of disorder in a many-body setting we show that here the dynamics is governed by an Anderson-Fock model, i.e. an Anderson model formulated on a lattice with sites corresponding to many-body Fock states. We first consider a one-dimensional atom chain in a limit which is described by a one-dimensional Anderson-Fock model with disorder on every other site, featuring both localized and delocalized states. We then illustrate the effect of disorder experimentally in a situation in which the system maps on a two-dimensional Anderson-Fock model on a trimmed square lattice. We observe a clear suppression of excitation propagation which we ascribe to the localization of the many-body wavefunctions in Hilbert space.

Introduction. Rydberg gases provide a versatile platform for studies of quantum few-body and many-body phenomena with applications ranging from quantum information processing [1] to simulations of complex condensed matter systems. The experimental degree of control has reached a stage which enables efficient entanglement creation [2] and implementation of quantum Ising models [3, 4]. This opens pathways towards probing magnetic structures [5–8] as well as the exploration of open many-body quantum systems [9–15].

Of particular interest is the so-called facilitation mechanism (or anti-blockade), where the excitation of an atom to a Rydberg state is strongly enhanced in the vicinity of an already excited atom [16, 17]. This effect is of broad relevance and exploited in the design of quantum gates [18, 19] as well as in protocols for dissipative quantum state preparation [6]. In the many-body context it effectuates an aggregation mechanism, where an initial Rydberg excitation seed triggers a dynamical growth of excitation clusters [18, 20–23] and it enables the implementation of kinetic constraints [12, 24, 25] thereby connecting to the physics of glass-forming substances [26–28].

Here we perform a theoretical and experimental study of the facilitated dynamics of Rydberg excitations in a one-dimensional array of optical tweezers. In a first experiment conducted with only two of them we establish that the uncertainty of the atomic positions introduces disorder which strongly affects excitation transfer between the atoms. To gain insight on how disorder affects the many-body context we theoretically consider firstly a regime of small disorder and strong interaction, which lends itself to a description through a one-dimensional Anderson model [29–31] defined on a reduced Hilbert space. Here, the disorder occurs on every other "site" and the corresponding amplitudes are correlated due to their dependence on the interatomic distances. Finally, we conduct an experiment where we probe the excitation dynamics in a linear array of eight tweezers and provide first evidence of a strong suppression of excitation propagation. We show that in the accessed parameter regime the physics is governed by an effective two-dimensional Anderson model on a trimmed square lattice and we interpret the absence of propagation in terms of localization of the wavefunction in the Hilbert space.

Rydberg lattice gas with disorder. We consider a chain of tight optical traps (tweezers), each loaded with a single atom [4, 32–34]. Figure 1(a) displays an example for two atoms. We label the Cartesian coordinates with an index $i = 1, 2, 3$, with the chain lying along direction 3. The average separation between contiguous traps is $\mathbf{r}_0 = (0, 0, r_0)$. We describe the Rydberg atoms as effective two-level systems [35] with the electronic ground state $|\downarrow\rangle$ and a Rydberg excited state (or "excitation") $|\uparrow\rangle$. In the following, we refer to the tensor products of $|\uparrow\rangle$ and $|\downarrow\rangle$ states as "Fock basis". The atoms are driven by laser light with Rabi frequency Ω, and detuning Δ. Excited ones interact via a van-der-Waals potential $V(|\mathbf{r}|) = C_6/|\mathbf{r}|^6$ [35, 36]. The Hamiltonian of the system reads

$$H = \sum_k \left[\frac{\Omega}{2} \sigma_k^x + \Delta n_k + \sum_{l>k} V(|\mathbf{r}_k - \mathbf{r}_l|) n_k n_l \right] \qquad (1)$$

where k, l are lattice indices, $\sigma_k^x = |\uparrow_k\rangle\langle\downarrow_k| + |\downarrow_k\rangle\langle\uparrow_k|$ and $n_k = |\uparrow_k\rangle\langle\uparrow_k|$. We express the k-th atom position as $\mathbf{r}_k = (k-1)\mathbf{r}_0 + \delta\mathbf{r}_k$. The displacements $\delta\mathbf{r}_k$ originate from the finite temperature T of the atoms and constitute

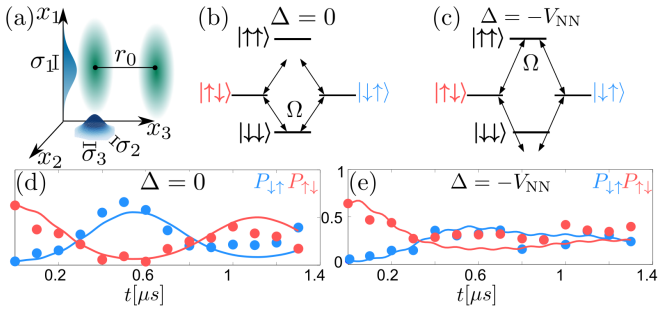

FIG. 1. Two-atom setting. (a) The harmonic traps are disposed in a line along $i = 3$ with average separation r_0 and widths σ_i. (b,c) Level structure for the two-atom case for the resonant ($\Delta = 0$) and facilitated ($\Delta = -V_{\rm NN}$) conditions respectively. The experimental data for the time evolution of the excitation probabilities $P_{\uparrow\downarrow}$, $P_{\downarrow\uparrow}$ are shown as full circles in panels (d,e). The data are averaged over at least 100 realizations of the disorder. The solid lines show numerical solutions of the dynamics obtained averaging over 30 realizations of the disorder. The experimental data here and in the following were obtained using ^{87}Rb atoms held at a temperature $T = 50$ μK in the traps with frequencies $\omega_1 = 2\pi \times 11$ kHz, $\omega_{2,3} = 2\pi \times 91.5$ kHz resulting in the position uncertainties $\sigma_1 = 1$ μm and $\sigma_{2,3} = 120$ nm. The internal levels are $|\downarrow\rangle = |5S_{1/2}, F = 2, M = 2\rangle$ and $|\uparrow\rangle = |100\, D_{3/2}, F = 3, M = 3\rangle$ with $r_0 = 14.2$ μm, $\Omega = 2\pi \times 1.25$ MHz, $C_6 = -2\pi \times 7.3 \times 10^7$ MHz μm^6. Consequently, $V_{\rm NN} = C_6/r_0^6 = -2\pi \times 8.9$ MHz and $|\delta V| \sim 2\pi \times 0.64$ MHz (all energies are in units of $\hbar$).

an intrinsic source of randomness. For sufficiently low T, the atoms, which are frozen during the experiment, occupy the harmonic part of the traps (with frequencies ω_i along $i = 1, 2, 3$). Hence, their distribution is approximately a Gaussian with widths $\sigma_i = \sqrt{k_B T/(m\omega_i^2)}$, with m the atomic mass [37]. Randomness enters Eq. (1) via the interaction term, which depends on the distances $d_{k,l} = |\mathbf{r}_{k+l} - \mathbf{r}_k| = |l\mathbf{r}_0 + \delta\mathbf{r}_{k+l} - \delta\mathbf{r}_k|$. Correspondingly, we introduce the energy displacements $\delta V_k \equiv V(d_{k,1}) - V(r_0)$. Note that these distances are not independently distributed: for instance, $d_{k+1,1}$ and $d_{k,1}$ both depend on $\mathbf{r}_{k+1}$, which generates correlation between them [37].

Two-atom dynamics and facilitation mechanism. We begin by illustrating the effect of the disorder in a two-atom setting. Considering first $\Delta = 0$ (see Fig. 1(b)), the two atomic states $|\uparrow\downarrow\rangle, |\downarrow\uparrow\rangle$ are resonant with $|\downarrow\downarrow\rangle$, while the interaction brings the state $|\uparrow\uparrow\rangle$ off resonance and thus decouples it from the dynamics. Since the disorder only acts on $|\uparrow\uparrow\rangle$, a dynamics starting from $|\downarrow\downarrow\rangle$, $|\uparrow\downarrow\rangle$, $|\downarrow\uparrow\rangle$, or combinations thereof, is not affected by it. In the experiment, after preparing the system in the $|\uparrow\downarrow\rangle$ state, the evolution thus resembles a coherent oscillation of the initial excitation between the atoms. This is shown in Fig. 1(d), where we display the excitation probabilities $P_{\uparrow\downarrow} = \langle n_1(1-n_2)\rangle$, $P_{\downarrow\uparrow} = \langle (1-n_1)n_2\rangle$ as functions

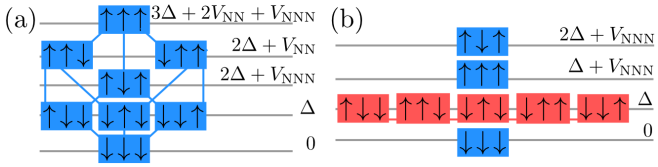

FIG. 2. Fock space structure for three atoms prior and after applying the facilitation condition. States with similar energy occupy the same row. (a) Internal structure of the Fock space. Linked states are connected by one spin flip. (b) Fock states spanning the reduced Hilbert space under facilitation conditions are shown in red (see text for details).

of time. The presence of the disorder becomes apparent instead when driving the system through the $|\uparrow\uparrow\rangle$ resonance. This is achieved by setting $\Delta = -V_{\rm NN}$ (Fig. 1(c)), the so-called "facilitation condition" [24, 38–41], where $V_{\rm NN} = V(r_0)$ is the nearest-neighbor interaction energy in the absence of disorder. Here, the amplitude of the oscillations of $P_{\downarrow\uparrow}$ and $P_{\uparrow\downarrow}$ is suppressed, see Fig. 1(e). This means that the displacements $\delta\mathbf{r}_1$, $\delta\mathbf{r}_2$ can be sufficiently large to bring the $|\uparrow\uparrow\rangle$ state off-resonance, hindering in turn the propagation of the initial excitation. Note that the initial state $|\uparrow\downarrow\rangle$ is obtained with non-unit probability due to experimental imperfections (see Supplemental Material [37] for details). We also refer to [4, 33] for further details on the experimental setting.

Generalization to many atoms. We investigate now the facilitated propagation of an excitation through a one-dimensional chain of atoms and first consider a simplified situation before addressing the parameter regime accessed by our experiment. The Hilbert space of our system can be depicted as a complex network of Fock states. Only states which differ by a single spin flip are connected by Hamiltonian (1) via the "flipping" ($\propto \Omega$) term. This is sketched in Fig. 2(a) for three atoms, where we label the states with their diagonal energies (i.e., their energies for $\Omega = 0$), dub $V_{\rm NNN} = V(2r_0)$ the next-nearest-neighbor interactions and assume we can neglect all terms $V(nr_0)$ for $n > 2$. In the following we fix the facilitation condition $\Delta = -V_{\rm NN}$ and we make a number of simplifying assumptions: (i) *large detuning* ($\Delta \gg \Omega$). This strongly suppresses unfacilitated transitions. (ii) *strong next-nearest neighbor blockade* ($V(2r_0) \gg \Omega, \delta V_k$). Interactions at distance $2r_0$ are supposed to be sufficiently strong to suppress transitions. In particular, we require this suppression to be much stronger than the one produced by the disorder. We also consider a tight confinement of the atoms, $\sigma_j \ll r_0$, such that, as in Fig. 1(e), the disorder can hinder, but not prevent transport entirely (i.e., $\delta V_k \lesssim \Omega$).

Under these conditions the states organize in layers with large energy gaps approximately of the order of $V_{\rm NNN}$ or Δ. Within each layer, however, states are now separated by considerably smaller differences δV_k. We thereby neglect connections between different layers and

retain only the intra-layer ones [see Fig. 2(a,b)].

We focus now on the highlighted (red) layer at energy Δ [Fig. 2(b)]. We recall first that (i) implies that spins cannot be flipped if they do not have a *single* excited neighbor. As a consequence, clusters of consecutive excitations can shrink or grow, but not merge or (dis)appear, i.e., the number $N_{\rm cl}$ of these clusters is conserved (see also the discussion in [37]). Condition (ii) implies instead that a spin next to two consecutive excitations cannot flip (e.g., $|\uparrow\uparrow\downarrow\rangle \leftrightarrow |\uparrow\uparrow\uparrow\rangle$ is forbidden); it then follows that the number $N_{\rm NNN}$ of excitation triples ($\uparrow\uparrow\uparrow$) is conserved. The red layer in Fig. 2(b) corresponds to $N_{\rm cl} = 1$, $N_{\rm NNN} = 0$ as it exclusively includes states with a single excitation or a single pair of neighboring ones; in the following, the former kind will be denoted by odd integers, $|2j-1\rangle \equiv |\downarrow_1 \dots \downarrow_{j-1}\uparrow_j\downarrow_{j+1} \dots \downarrow_L\rangle$ $(j = 1 \dots L)$ whereas the latter by even integers, $|2j\rangle \equiv |\downarrow_1 \dots \downarrow_{j-1}\uparrow_j\uparrow_{j+1}\downarrow_{j+2} \dots \downarrow_L\rangle$ $(j = 1 \dots L-1)$. The dynamics restricted to this layer can be described by a one-dimensional Anderson model [29]. In fact, the Hamiltonian connects these states sequentially $(\dots |2j-1\rangle \leftrightarrow |2j\rangle \leftrightarrow |2j+1\rangle \dots)$, taking the form of a tight-binding model with sites labeled by $b = 1 \dots 2L-1$ and a random potential $h_b = (1+(-1)^b)\delta V_{b/2}/\Omega$ acting only on even ones. In this restricted space H can be recast as [37]

$$H_{\rm A} = \frac{\Omega}{2}\sum_{b=1}^{2L-2}\Big[|b\rangle\langle b+1| + |b+1\rangle\langle b| + h_b\,|b\rangle\langle b|\Big]. \quad (2)$$

The two main differences to the "canonical" Anderson model lie in the absence of disorder on odd sites and the fact that the h_b are identically distributed, but *not independent random variables*. In order to distinguish it from a standard Anderson model defined in real space, i.e., on a physical lattice, in the following we shall call it *Anderson-Fock model*.

Localization in the 1D Anderson-Fock model. Our analysis — analogously to the "canonical" case — focuses on the eigenvectors $|\psi_n\rangle$ of H_A. In the Fock basis, we distinguish between *localized* states whose amplitude $|\langle b|\psi_n\rangle|$ is concentrated within a region of width l and decays exponentially $\sim \mathrm{e}^{-r/l}$ with the distance r from it, and *delocalized* states which are instead extended and do not show exponentially-suppressed tails. Equivalently, one can introduce the Lyapunov exponent $\gamma = l^{-1}$ [42, 43]. Wavefunctions with $\gamma > 0$ are localized, whereas $\gamma = 0$ denotes delocalization. We emphasize that the Lyapunov exponent, as a function of the energy E, only depends on the distribution of the disorder, and not on the specific realizations thereof [44]. In Fig. 3 we report a numerical determination of γ for a chain of length $L = 25000$ sites. We provide details of these computations in [37]. We find that γ is positive $\forall E \neq 0$, while $\gamma(E=0) = 0$, signaling the presence of a delocalized state. The asymmetric shape originates from

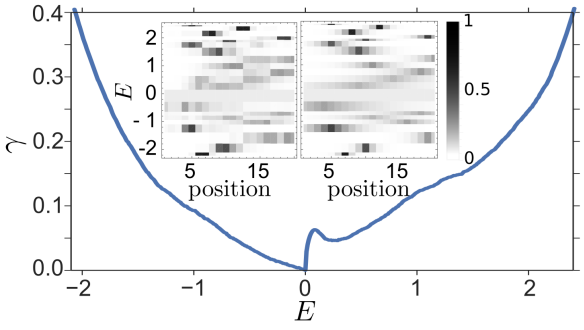

FIG. 3. Lyapunov exponent for the one-dimensional Anderson-Fock model. All data shown in this figure are obtained with the same parameters given in Fig. 1. In the main figure we report the Lyapunov exponent as a function of the energy E (measured in units of $\Omega/2$). The inset shows a comparison between the shapes of the wave functions obtained from a numerical reconstruction (left panel) and from the corresponding prediction associated to the Lyapunov exponent (right panel) for a chain of $L = 20$ sites and a specific realization of the disorder. In the right panel the envelopes $\propto \exp\left[-4\gamma(E)\,|k - k_{\rm max}(E)|\right]$ are centered at the position $k_{\rm max}(E)$ at which the corresponding set of excitation probabilities in the left panel reaches its maximum. The factor 4 in the exponent stems from considering probabilities instead of amplitudes and the fact that the length of the atomic chain is about half the one in Fock space.

an asymmetry of the distribution of energy displacements between positive and negative values [37]. In the inset we compare our Lyapunov exponent results with a numerical simulation of a system of size $L = 20$ (for a randomly chosen realization of the disorder). This shows that the Lyapunov exponent provides a reasonably reliable prediction already for relatively small system sizes.

Note, that $E = 0$ is always — independently of the realization of disorder — an eigenvalue of $H_{\rm A}$ and corresponds to the (delocalized) wavefunction $|\psi_0\rangle = (1/\sqrt{L})\sum_b \sin(\pi b/2)\,|b\rangle$, which has nonvanishing components only on states not affected by the disorder. This is in contrast with the standard Anderson model [29], which features full localization, and is instead reminiscent of related works on one dimensional models: the random dimer model [42, 45–48] and the Anderson model in the presence of correlated disorder [43], both exhibiting delocalized states in the spectrum.

Localization in the 2D Anderson-Fock model. Moving away from this simplified discussion we now analyze an experiment conducted in a chain of 8 atoms. We monitor the local densities $\langle n_k(t)\rangle$ starting from a single excitation $|\psi_{\rm in}\rangle = |\uparrow\downarrow\downarrow\downarrow\downarrow\downarrow\downarrow\downarrow\rangle$. The result is displayed in Fig. 4(a) and no appreciable propagation beyond the second site is observed, signaling a strong suppression of transport. As shown in the following, this can again be ascribed to the fact that the eigenstates are localized, although via a slightly modified theoretical description.

Solving Hamiltonian (1) in the presence of disorder,

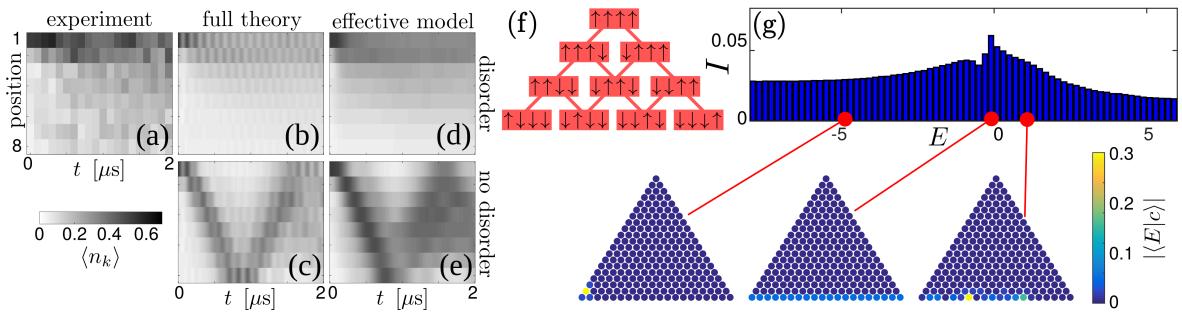

FIG. 4. Eight-atom experiment and two-dimensional Anderson-Fock model. (a) Experimental data for the dynamics of the site-resolved excitation probability averaged over more than 100 realizations. Here, $|\uparrow\rangle = |56D_{3/2}, F = 3, M = 3\rangle$, $r_0 = 4.1$ μm, $\Omega = 2\pi \times 2.1$ MHz, $\Delta = -V_{\rm NN} = -2\pi \times 8.4$ MHz and $|\delta V| \sim 2\pi \times 2.1$ MHz (in units of $\hbar$). The data are compared with numerical data from exact diagonalization of the Hamiltonian (b,c), and the 2D Anderson-Fock model (d,e), with and without disorder. Disorder averages are made over 100 realizations. In the absence and for low disorder ($|\delta V| \lesssim 2\pi \times 0.4$ MHz), excitations still propagate ballistically. (f) Lattice structure of the effective model for $L = 4$ atoms and $N_{\rm cl} = 1$. (g) Inverse participation ratio I as a function of the energy E (measured in units of $\Omega/2$) for a chain of $L = 20$ atoms. The amplitude of the wave function (projecting $|E\rangle$ on the Fock basis $|c\rangle$) is reported for four representative states on a lattice whose structure follows the one shown in panel (f). From left to right they display: a state localized in both Fock space and real space, the special state $|\psi_0\rangle$ and a similar state found for small $E > 0$ (see text for details).

Fig. 4(b), we find localization, in good agreement with the experimental data. The case without randomness, studied only numerically (Fig. 4(c)), features instead propagation. In our experiment condition (ii) (i.e., $V_{\rm NNN} \gg \delta V_k$) is not satisfied. It is thereby possible to grow clusters beyond the two-excitation limit. This breaks the chain-like structure obtained from the simplified description [Fig. 2(b)]. Instead it gives rise — when considering a single cluster ($N_{\rm cl} = 1$) — to a two-dimensional square lattice with $N = L(L+1)/2$ sites. This structure, previously discussed in Ref. [49], is sketched in Fig. 4(f) for four atoms. We remark that the two bottommost rows correspond precisely to the previous one-dimensional chain. The dynamics on this "triangle" of states is described by a 2D tight-binding Anderson-Fock model similar to Eq. (2) (see [37] for the derivation). As shown in Fig. 4(d)-(e) the solutions of this effective model agree well with that of the full Hamiltonian.

The observed inhibition of excitation propagation stems from the localization of the many-body eigenstates $|E\rangle$ on the restricted Fock basis $|c\rangle$. We quantify the degree of localization by means of the inverse participation ratio (IPR) $I = (N \sum_c |\langle E|c\rangle|^4)^{-1}$ [50]. As a measure of localization, the IPR can be easily tested on the two limiting cases: for a state $|E\rangle$ uniformly distributed on the basis ($|\langle E|c\rangle| = 1/\sqrt{N}$) one finds the maximal value $I = 1$, whereas for a completely localized state, namely $|E\rangle \equiv |\bar{c}\rangle$ corresponding to a single Fock state $|\bar{c}\rangle$, one has $I = 1/N$. A numerical study of I for $L = 20$ atoms and the parameter set employed in the experiment is reported in Fig. 4(g), where for every realization of the disorder the spectrum is calculated via exact diagonalization. The IPR is then computed for each energy eigenvector and a first average is calculated among levels which end up in the same bin of the histogram. A second average is then applied over all the considered realizations. In general, we observe that the IPR remains rather low on the entire spectrum ($I < 0.1$), signaling that the parameters are in the localized phase. The form of the IPR indicates the presence of strongly localized states at large energies (both positive and negative), while eigenstates at smaller energies are slightly more spread-out. The central peak links to the presence of the state $|\psi_0\rangle = |E = 0\rangle$ encountered above, which is still an exact eigenstate, but only occupies the bottommost row [see example in Fig. 4(g)], its IPR being $I = L/N = 2/(L+1)$.

It is important to remark that despite the mapping onto a single particle Anderson problem in Fock space, the system is in fact interacting in real space and does not reduce in general to a non-interacting Anderson problem. In particular, rephrasing the dynamics in terms of domain wall degrees of freedom [51, 52] does not yield free particles [37].

Outlook. The Rydberg excitation dynamics in detuned optical tweezer arrays is governed by certain classes of tight binding Anderson models featuring inhibited excitation transport, the simplest one being a 1D Anderson-Fock model with disorder on every other site. Currently accessed experimental parameter regimes feature a 2D manifestation of an Anderson-Fock model with correlated disorder, whose behavior is largely unexplored. The presented system opens possibilities for studies of multidimensional Anderson models, where the dimensionality is twice the number of excitation clusters. This connection may shed light on how Fock space localization influences real space localization, which is a subtle and interesting open problem in the context of many-body localization

[53, 54], which started to be addressed experimentally only very recently [55, 56].

Acknowledgments. IL thanks Juan P. Garrahan for fruitful discussions. The research leading to these results has received funding from European Research Council under the European Union's Seventh Framework Programme (FP/2007-2013) / ERC Grant Agreement No. 335266 (ESCQUMA), the EU-FET Grant No. 512862 (HAIRS), the H2020-FETPROACT-2014 Grant No.640378 (RYSQ), and EPSRC Grant No. EP/M014266/1 and by the Région Ile-de-France in the framework of DIM Nano-K.

[1] M. Saffman, T. G. Walker, and K. Mølmer, Rev. Mod. Phys. **82**, 2313 (2010).
[2] Y.-Y. Jau, A. Hankin, T. Keating, I. Deutsch, and G. Biedermann, Nature Physics **12**, 71 (2016).
[3] P. Schauß, J. Zeiher, T. Fukuhara, S. Hild, M. Cheneau, T. Macrì, T. Pohl, I. Bloch, and C. Groß, Science **347**, 1455 (2015).
[4] H. Labuhn, D. Barredo, S. Ravets, S. de Léséleuc, T. Macrì, T. Lahaye, and A. Browaeys, Nature **534**, 667 (2016).
[5] T. E. Lee, H. Häffner, and M. C. Cross, Phys. Rev. A **84**, 031402 (2011).
[6] A. W. Carr and M. Saffman, Phys. Rev. Lett. **111**, 033607 (2013).
[7] M. Hoening, W. Abdussalam, M. Fleischhauer, and T. Pohl, Phys. Rev. A **90**, 021603 (2014).
[8] R. M. W. van Bijnen and T. Pohl, Phys. Rev. Lett. **114**, 243002 (2015).
[9] H. Weimer, Phys. Rev. A **91**, 063401 (2015).
[10] M. Marcuzzi, M. Buchhold, S. Diehl, and I. Lesanovsky, Phys. Rev. Lett. **116**, 245701 (2016).
[11] D. C. Rose, K. Macieszczak, I. Lesanovsky, and J. P. Garrahan, arXiv preprint arXiv:1607.06780 (2016).
[12] B. Everest, M. Marcuzzi, J. Garrahan, and I. Lesanovsky, arXiv:1602.05839 (2016).
[13] V. R. Overbeck, M. F. Maghrebi, A. V. Gorshkov, and H. Weimer, arXiv preprint arXiv:1606.08863 (2016).
[14] N. Šibalić, C. G. Wade, C. S. Adams, K. J. Weatherill, and T. Pohl, Phys. Rev. A **94**, 011401 (2016).
[15] S. Helmrich, A. Arias, and S. Whitlock, arXiv:1605.08609.
[16] C. Ates, T. Pohl, T. Pattard, and J. M. Rost, Phys. Rev. Lett. **98**, 023002 (2007).
[17] T. Amthor, C. Giese, C. S. Hofmann, and M. Weidemüller, Phys. Rev. Lett. **104**, 013001 (2010).
[18] M. Gärttner, K. P. Heeg, T. Gasenzer, and J. Evers, Phys. Rev. A **88**, 043410 (2013).
[19] R. C. Teixeira, C. Hermann-Avigliano, T. L. Nguyen, T. Cantat-Moltrecht, J. M. Raimond, S. Haroche, S. Gleyzes, and M. Brune, Phys. Rev. Lett. **115**, 013001 (2015).
[20] I. Lesanovsky and J. P. Garrahan, Phys. Rev. A **90**, 011603 (2014).
[21] H. Schempp, G. Günter, M. Robert-de Saint-Vincent, C. S. Hofmann, D. Breyel, A. Komnik, D. W. Schönleber, M. Gärttner, J. Evers, S. Whitlock, and M. Weidemüller, Phys. Rev. Lett. **112**, 013002 (2014).
[22] A. Urvoy, F. Ripka, I. Lesanovsky, D. Booth, J. P. Shaffer, T. Pfau, and R. Löw, Phys. Rev. Lett. **114**, 203002 (2015).
[23] C. Simonelli, M. M. Valado, G. Masella, L. Asteria, E. Arimondo, D. Ciampini, and O. Morsch, arXiv preprint arXiv:1602.01257 (2016).
[24] I. Lesanovsky and J. P. Garrahan, Phys. Rev. Lett. **111**, 215305 (2013).
[25] M. M. Valado, C. Simonelli, M. D. Hoogerland, I. Lesanovsky, J. P. Garrahan, E. Arimondo, D. Ciampini, and O. Morsch, Phys. Rev. A **93**, 040701 (2016).
[26] J. P. Garrahan and D. Chandler, Proceedings of the National Academy of Sciences **100**, 9710 (2003), http://www.pnas.org/content/100/17/9710.full.pdf.
[27] J. P. Garrahan, P. Sollich, and C. Toninelli, arXiv:1009.6113 (2010).
[28] G. Biroli and J. P. Garrahan, J. Chem. Phys. **138**, 12A301 (2013).
[29] P. W. Anderson, Phys. Rev. **109**, 1492 (1958).
[30] N. Mott and W. Twose, Advances in Physics **10**, 107 (1961).
[31] K. Ishii, Progress of Theoretical Physics Supplement **53**, 77 (1973).
[32] F. Nogrette, H. Labuhn, S. Ravets, D. Barredo, L. Béguin, A. Vernier, T. Lahaye, and A. Browaeys, Phys. Rev. X **4**, 021034 (2014).
[33] H. Labuhn, S. Ravets, D. Barredo, L. Béguin, F. Nogrette, T. Lahaye, and A. Browaeys, Phys. Rev. A **90**, 023415 (2014).
[34] D. Barredo, H. Labuhn, S. Ravets, T. Lahaye, A. Browaeys, and C. S. Adams, Phys. Rev. Lett. **114**, 113002 (2015).
[35] R. Löw, H. Weimer, J. Nipper, J. B. Balewski, B. Butscher, H. P. Büchler, and T. Pfau, J. Phys. B: At. Mol. Opt. Phys. **45**, 113001 (2012).
[36] L. Béguin, A. Vernier, R. Chicireanu, T. Lahaye, and A. Browaeys, Phys. Rev. Lett. **110**, 263201 (2013).
[37] See Supplemental Material [url], which includes Refs. [42-44,49,57].
[38] C. Ates, T. Pohl, T. Pattard, and J. M. Rost, Phys. Rev. Lett. **98**, 023002 (2007).
[39] T. Amthor, C. Giese, C. S. Hofmann, and M. Weidemüller, Phys. Rev. Lett. **104**, 013001 (2010).
[40] I. Lesanovsky and J. P. Garrahan, Phys. Rev. A **90**, 011603 (2014).
[41] M. M. Valado, C. Simonelli, M. D. Hoogerland, I. Lesanovsky, J. P. Garrahan, E. Arimondo, D. Ciampini, and O. Morsch, Phys. Rev. A **93**, 040701 (2016).
[42] F. M. Izrailev, T. Kottos, and G. P. Tsironis, Phys. Rev. B **52**, 3274 (1995).
[43] F. M. Izrailev and A. A. Krokhin, Phys. Rev. Lett. **82**, 4062 (1999).
[44] H. Furstenberg and H. Kesten, Ann. Math. Statist. **31**, 457 (1960).
[45] J. C. Flores, Journal of Physics: Condensed Matter **1**, 8471 (1989).
[46] D. H. Dunlap, H.-L. Wu, and P. W. Phillips, Phys. Rev. Lett. **65**, 88 (1990).
[47] A. Bovier, Journal of Physics A: Mathematical and General **25**, 1021 (1992).
[48] S. De Bièvre and F. Germinet, Journal of Statistical

Physics **98**, 1135 (2000).
[49] M. Mattioli, A. W. Glätzle, and W. Lechner, New Journal of Physics **17**, 113039 (2015).
[50] R. J. Bell and P. Dean, Discuss. Faraday Soc. **50**, 55 (1970).
[51] J.-S. Lee and A. K. Khitrin, Phys. Rev. A **71**, 062338 (2005).
[52] G. B. Furman, S. D. Goren, J.-S. Lee, A. K. Khitrin, V. M. Meerovich, and V. L. Sokolovsky, Phys. Rev. B **74**, 054404 (2006).
[53] I. V. Gornyi, A. D. Mirlin, and D. G. Polyakov, Phys. Rev. Lett. **95**, 206603 (2005).
[54] D. Basko, I. Aleiner, and B. Altshuler, Annals of Physics **321**, 1126 (2006).
[55] M. Schreiber, S. S. Hodgman, P. Bordia, H. P. Lüschen, M. H. Fischer, R. Vosk, E. Altman, U. Schneider, and I. Bloch, Science **349**, 842 (2015).
[56] J. Smith, A. Lee, P. Richerme, B. Neyenhuis, P. W. Hess, P. Hauke, M. Heyl, D. A. Huse, and C. Monroe, Nature Physics (2016), 10.1038/nphys3783.
[57] C. da Fonseca and J. Petronilho, Linear Algebra and its Applications **325**, 7 (2001).

Facilitation dynamics and localization phenomena in Rydberg lattice gases with position disorder: Supplemental Material

Matteo Marcuzzi,[1,2] Jiří Minář,[1,2] Daniel Barredo,[3] Sylvain de Léséleuc,[3] Henning Labuhn,[3] Thierry Lahaye,[3] Antoine Browaeys,[3] Emanuele Levi,[1,2] and Igor Lesanovsky[1,2]

[1]*School of Physics and Astronomy, University of Nottingham, Nottingham, NG7 2RD, United Kingdom*
[2]*Centre for the Mathematics and Theoretical Physics of Quantum Non-equilibrium Systems, University of Nottingham, Nottingham, NG7 2RD, United Kingdom*
[3]*Laboratoire Charles Fabry, Institut d'Optique Graduate School, CNRS, Université Paris-Saclay, 91127 Palaiseau cedex, France*

I. APPROXIMATE GAUSSIAN DISTRIBUTION OF THE ATOMIC POSITIONS

Here we recall how the Gaussian distribution of the atomic positions arises. As a first approximation, we assume the motional degrees of freedom to be classical, so that we can describe the position of the atom by the Boltzmann distribution $f(\mathbf{r},\mathbf{p}) = \exp\left(-\beta H_{\rm motion}(\mathbf{r},\mathbf{p})\right)$. For low enough temperatures, the atoms have only access to the harmonic part of the potential and $H_{\rm motion}(\mathbf{r},\mathbf{p}) \approx \sum_i p_i^2/(2m) + (m/2)\sum_i \omega_i^2 r_i^2$. The distribution of the positions $p_{\rm pos} = (\int \mathrm{d}^3p\, f)/(\int \mathrm{d}^3p\, \mathrm{d}^3r\, f)$ can be read off directly and is a Gaussian with zero mean and variances $\sigma_i^2 = 1/(m\omega_i^2\beta)$. The complete three-dimensional distribution is then simply a product of $p_{\rm pos}(x_i)$ along the three directions. For an atom in a trap centered at position $k\mathbf{r}_0 = (0,0,kr_0)$ with k an integer, it is straightforwardly generalized to

$$p^{(k)}_{\rm pos}(\mathbf{r}) = \frac{1}{(2\pi)^{3/2}\,\sigma_1\sigma_2\sigma_3}\mathrm{e}^{-\frac{r_1^2}{2\sigma_1^2}-\frac{r_2^2}{2\sigma_2^2}-\frac{(r_3-kr_0)^2}{2\sigma_3^2}}. \tag{S1}$$

We remark that the indices in the expression above distinguish between Cartesian components only, e.g r_1 and r_2 are the components along x and y of the same atomic position. In the following, whenever necessary to display both, the trap index will always appear before the component one, e.g., $r_{k,i}$ is the i-th component of the k-th atom's position.

II. CORRELATION OF THE DISTANCES AND TYPICAL INTERACTION DISPLACEMENTS

In this section we explain how the independent atomic positions lead to correlated inter-atomic distances and, in turn, to correlated energy fluctuations. We comment on the respective probability distributions.

In our numerical simulations, each atomic position $\mathbf{r}_k$ is independently generated according to the distribution (S1) relative to its own trap. As explained in the main text, the nearest-neighbour differences, $\mathbb{d}_k \equiv \mathbf{d}_{k,1} = \mathbf{r}_{k+1} - \mathbf{r}_k = (\mathbb{d}l^1_k, \mathbb{d}l^2_k, \mathbb{d}l^3_k)$ are not independent - for example, both $\mathbb{d}_1$ and $\mathbb{d}_2$ depend on the position of the second atom. The joint distribution of $\mathbb{d}_k$s can be obtained from the atomic positions distribution as

$$\begin{aligned} p_{\rm diff}(\mathbb{d}_1,\dots,\mathbb{d}_{L-1}) &= \int \left[\prod_{k=1}^{L} \mathrm{d}^3r_k\, p^{(k)}_{\rm pos}(\mathbf{r}_k)\right]\left[\prod_{k'=1}^{L-1}\delta^{(3)}\left(\mathbb{d}_{k'} - (\mathbf{r}_{k'+1}-\mathbf{r}_{k'})\right)\right] = \\ &= \left[\frac{1}{\sqrt{L}\left(\sqrt{2\pi}\right)^{L-1}}\right]^3 \left(\sigma_1\sigma_2\sigma_3\right)^{1-L}\mathrm{e}^{-\frac{1}{2}\sum_{k,q}\left[\frac{1}{\sigma_1^2}\mathbb{d}l^1_k A_{kq}\mathbb{d}l^1_q + \frac{1}{\sigma_2^2}\mathbb{d}l^2_k A_{kq}\mathbb{d}l^2_q + \frac{1}{\sigma_3^2}(\mathbb{d}l^3_k - r_0)A_{kq}(\mathbb{d}l^3_q - r_0)\right]}, \end{aligned} \tag{S2}$$

where $A_{kq} = L - \max(k,q) - (L-k)(L-q)/L = (L-\max(k,q))\min(k,q)/L$ is a symmetric real matrix. From here, one can determine the correlation properties of the distances: the correlation matrix $C = A^{-1}$ is a tridiagonal matrix [42]

$$C = \begin{pmatrix} 2 & -1 & 0 & 0 & \\ -1 & 2 & -1 & 0 & \\ 0 & -1 & 2 & -1 & \cdots \\ 0 & 0 & -1 & 2 & \\ & & \vdots & & \ddots \end{pmatrix} \tag{S3}$$

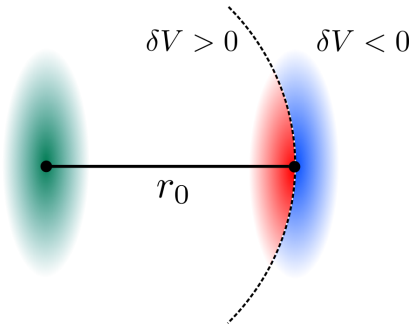

FIG. S1. **Asymmetry of the energy displacements.** Here an excitation is present in the center of the leftmost trap (in green). The dashed line indicates the facilitation shell, i.e., the sphere of points where $V(r_0) = -\Delta$. For repulsive interactions, the red portion of the second trap corresponds to the domain where the energy displacement is positive ($\delta V > 0$), whereas the opposite ($\delta V < 0$) holds for the blue one. It is then apparent that the volume covered by the blue portion is larger than the volume of the red one, yielding the mentioned bias towards negative values.

implying e.g. $\langle \mathbb{d}_k^3 \mathbb{d}_q^3 \rangle_c \equiv \langle \mathbb{d}_k^3 \mathbb{d}_q^3 \rangle - \langle \mathbb{d}_k^3 \rangle \langle \mathbb{d}_q^3 \rangle = \sigma_3^2 \left(2\delta_{k,q} - \delta_{k,q+1} - \delta_{k,q-1}\right)$. It confirms the expected result, namely that contiguous distances are (anti-)correlated. This comes from the simple fact that, considering three atoms, moving the middle atom closer to the first one brings it further away from the last one.

As mentioned in the main text, the asymmetric profiles of both the Lyapunov exponent (for the 1D case) and the inverse participation ratio (for the 2D case), stem from the asymmetry of the distribution $p_{\rm int}(\delta V)$ of energy displacements. For anisotropic traps ($\sigma_i \neq \sigma_j$) there is no closed formula for $p_{\rm int}$. However, considering for instance repulsive interactions ($V(r) > 0$), the bias towards negative values ($\delta V < 0$) can still be understood simply by analyzing the geometry of the setup: in Fig. S1 we display two neighboring traps. The facilitation radius r_0 corresponds to the distance at which the detuning Δ exactly cancels the interaction $V(r_0)$ and thus separates the regime $\delta V > 0$ (inside, $\mathbb{d} < r_0$, red area in the figure) from $\delta V < 0$ (outside, $\mathbb{d} > r_0$, blue area in the figure). It then becomes apparent that the former includes a smaller portion of the second trap than the latter. In other words, setting as a first approximation the first atom in the center of its trap, the placement of the second one will more likely yield a distance $\mathbb{d} > r_0$ than the converse. For attractive interactions, the signs change and the bias will be towards positive values.

The typical energy displacement can also be estimated by simple considerations: taking two neighboring atoms at average separation $\mathbf{r}_0 = (0, 0, r_0)$ and standard deviation (of the distance between them) $\overline{\delta r} = \sqrt{\langle \mathbb{d}^2 \rangle - \langle \mathbb{d} \rangle^2} \approx \sqrt{2}\sigma_3$, we define

$$\overline{\delta V} = \left| \frac{\partial V}{\partial r} \right| \overline{\delta r} = 6 \left| V(r_0) \right| \frac{\overline{\delta r}}{r_0}. \tag{S4}$$

We emphasize that we only include here the contribution σ_3, which is the only one acting to first order in $\sigma_{1,2,3}/\mathbb{d}$. This yields a reasonable lower bound on $\overline{\delta V}$.

For the set of parameters used in the two-atoms experiment ($\sigma_3 = 0.12\,\mu$m, $r_0 = 14.2\ \mu$m, $V(r_0)/\hbar = 2\pi \times 8.9\,$MHz) we find $\overline{\delta V}/\hbar \approx 2\pi \times 0.64\,$MHz. For the eight-atoms experiment ($\sigma_3 = 0.12\,\mu$m, $r_0 = 4.1\ \mu$m, $V(r_0)/\hbar = 2\pi \times 8.4\,$MHz) we obtain $\overline{\delta V}/\hbar \approx 2\pi \times 2.1\,$MHz. This value is to be compared with the Rabi frequency $\Omega/\hbar \approx 2\pi \times 2.1\,$MHz and confirms the relevance of the disorder for the propagation of excitations in this setup.

III. LOCALIZATION IN THE 1D ANDERSON-FOCK MODEL.

In this section, for simplicity we measure all energies and (inverse) times in units of (half) the Rabi frequency, setting $\Omega = 2$. We approach the problem with a transfer matrix formalism: expressing the quantum state in the restricted Fock basis $|b\rangle$, $|\psi\rangle = \sum_b a_b |b\rangle$, the Schrödinger equation $H_{\rm A} |\psi\rangle = E |\psi\rangle$ reduces to the recursion equation

$$\begin{pmatrix} a_{b+1} \\ a_b \end{pmatrix} = \begin{pmatrix} E - h_b & -1 \\ 1 & 0 \end{pmatrix} \begin{pmatrix} a_b \\ a_{b-1} \end{pmatrix} \equiv M_b \begin{pmatrix} a_b \\ a_{b-1} \end{pmatrix}, \tag{S5}$$

where $M_b = M_b(E)$ is an energy-dependent transfer matrix which progressively reconstructs the wave function amplitudes from left to right. The values of E belonging to the spectrum of the Hamiltonian are identified by the boundary conditions $a_{2L} = a_0 = 0$.

The localization length l can be expressed in terms of the Lyapunov exponent [38,39],

$$\gamma(E) \equiv \lim_{n\to\infty} \frac{1}{n} \log \left\| \prod_{b=n}^{1} M_b(E) \right\|_{\text{op}} \equiv l^{-1}, \tag{S6}$$

where $\|M\|_{\text{op}} = \sup_{\vec{x}} \|M\vec{x}\| / \|\vec{x}\|$ is the operator norm, with $\vec{x}$ denoting a generic vector and $\|\cdot\|$ the Euclidean norm (for the existence of the limit see [40]).

IV. HILBERT SPACE REDUCTIONS AND RESTRICTED HAMILTONIANS

A. Derivation of the effective Hamiltonians

Here we provide the detailed derivation of the effective 1D and 2D Hamiltonians. For the reader's convenience, we recall here from the main text the original Hamiltonian

$$H = \sum_k \left[\frac{\Omega}{2}\sigma_k^x + \Delta n_k + \sum_{l>k} V(|\mathbf{r}_k - \mathbf{r}_l|) n_k n_l \right] \tag{S7}$$

of the model. For simplicity, we are going to neglect all interactions beyond next-nearest neighbors (NNN) (for the parameters above, e.g., $|V(3r_0)/\Omega| \sim 10^{-3}$), so that the second sum above can be restricted to $l = k+1, k+2$. Second, the relative displacement between NNNs is suppressed by a factor $2^6 = 64$ with respect to the noise between nearest neighbors and can therefore also be discarded. After these basic approximations, H takes the form

$$\begin{aligned} H &= \sum_k \Big[\frac{\Omega}{2}\sigma_k^x + \Delta n_k + (V_{\text{NN}} + \delta V_k) n_k n_{k+1} + + V_{\text{NNN}} n_k n_{k+2} \Big] \\ &= \sum_k \Big[\frac{\Omega}{2}\sigma_k^x + \Delta n_k (1 - n_{k+1}) + \delta V_k n_k n_{k+1} + + V_{\text{NNN}} n_k n_{k+2} \Big] \end{aligned} \tag{S8}$$

where we used the facilitation constraint $V_{\text{NN}} = -\Delta$. Note that the sum runs over $k = 1 \dots L$ and, for later convenience, we fix four auxiliary variables $n_{-1} = n_0 = n_{L+1} = n_{L+2} \equiv 0$. We now enforce condition (i) $\Delta \gg \Omega$. This implies that spin flips are strongly suppressed if not in the presence of a single excited neighbor; we further approximate our Hamiltonian by making this a hard constraint. In other words, the transitions $|\downarrow\downarrow\downarrow\rangle \leftrightarrow |\downarrow\uparrow\downarrow\rangle$ and $|\uparrow\downarrow\uparrow\rangle \leftrightarrow |\uparrow\uparrow\uparrow\rangle$ are prohibited. If we now define a "cluster" as an uninterrupted sequence of $\uparrow$ spins (for instance, the state $|\downarrow \boxed{\uparrow\uparrow} \downarrow \boxed{\uparrow} \downarrow \boxed{\uparrow\uparrow\uparrow}\rangle$ has three highlighted clusters), we see that these structures cannot appear or disappear, nor can they merge or split. Hence, as pointed out in [41] as well, the number N_{cl} of these clusters is conserved. In particular, having fixed $n_{L+1} = 0$, the number of clusters corresponds to the number of right kinks $|\uparrow\downarrow\rangle$, i.e., $N_{\text{cl}} = \sum_{k=1}^{L} n_k(1 - n_{k+1})$. The Hamiltonian now reads

$$H = \Delta N_{\text{cl}} + \sum_k \Big[\frac{\Omega}{2}\sigma_k^x P_k^{(i)} + \delta V_k n_k n_{k+1} + V_{\text{NNN}} n_k n_{k+2} \Big] \tag{S9}$$

with the projector $P_k^{(i)} = n_{k-1} + n_{k+1} - 2n_{k-1}n_{k+1}$. If we consider now the special case $N_{\text{cl}} = 1$, we notice that the states with a single cluster can be labeled by two indices: the starting position of the cluster ($\mu = 1 \dots L$) and the ending one $\nu = \mu \dots L$. In order to enforce the condition $\nu \geq \mu$ and avoid spurious boundary terms, we formally use the projector $\Theta\,|\mu,\nu\rangle = \theta(\nu-\mu)\theta(\mu)\theta(\nu)\theta(L-\mu)\theta(L-\nu)\,|\mu,\nu\rangle$ on the valid states, where $\theta(x)$ is the Heaviside step function ($\theta(x \geq 0) = 1$ and $\theta(x < 0) = 0$). Since clusters only grow/shrink at the edges, the Hamiltonian can be recast in the form

$$H_B = \Omega\,\Theta H_B' \Theta \quad \text{with} \tag{S10a}$$

$$\begin{aligned} H_B' = \sum_{\mu,\nu=1}^{L} \Big[&\frac{1}{2} \left(|\mu,\nu\rangle\langle\mu+1,\nu| + |\mu,\nu\rangle\langle\mu,\nu+1| + h.c. \right) + \\ &\left(\delta v_{\mu\nu} + (\nu-\mu-2)\theta(\nu-\mu-2)\frac{V_{\text{NNN}}}{\Omega} \right) |\mu,\nu\rangle\langle\mu,\nu| \Big], \end{aligned} \tag{S10b}$$

where $\delta v_{\mu\nu} = \sum_{k=\mu}^{\nu-1} \delta V_k/\Omega$ and for simplicity we subtracted the additive constant Δ. In this notation, one can regard H_B as a hopping Hamiltonian on half a square lattice (since we take $\nu \geq \mu$), as reported in the main text. Each site feels a random potential $\delta v_{\mu\nu}$ and a deterministic one originating from the NNN interactions (provided of course, that there are more than two $\uparrow$ spins in the cluster). It is therefore reminiscent of a 2D Anderson problem, the main difference being in the peculiar form of the noise, which appears as the sum of at most $L-1$ random variables and makes it non-trivially correlated between different sites.

The 1D Anderson-Fock model we introduce in our main text is obtained when condition (ii) $V_{\rm NNN} \gg \Omega$ also holds. By approximating this as a hard constraint (i.e., assuming the limit $V_{\rm NNN}/\Omega \to \infty$) the number of next-nearest-neighboring excitations $N_{\rm NNN}$ becomes a conserved quantity. The Hamiltonian then reads

$$H = \Delta N_{\rm cl} + N_{\rm NNN} V_{\rm NNN} + \sum_k \Big[\frac{\Omega}{2} \sigma_k^x P_k^{(i)} P_k^{(ii)} + \delta V_k n_k n_{k+1} \Big], \tag{S11}$$

with the additional projector $P_k^{(ii)} = (1-n_{k-2})(1-n_{k+2})$. Note that under these conditions spins neighboring a pair of excitations cannot flip (e.g., $|\uparrow\uparrow\downarrow\rangle \leftrightarrow |\uparrow\uparrow\uparrow\rangle$ is suppressed). Similarly, different clusters cannot grow to a distance smaller than two now (i.e., transitions such as $|\uparrow\downarrow\downarrow\uparrow\rangle \leftrightarrow |\uparrow\uparrow\downarrow\uparrow\rangle$ are prohibited as well). This means that any longer-than-two cluster is a stable local configuration (i.e., invariant under the dynamics generated by (S11)) which cuts the chain of atoms in two dynamically-disconnected parts. Each of these parts can be read as a subsystem subject to the same Hamiltonian (S11) but with lower $N_{\rm NNN}$. Therefore, the analysis can be restricted, without conceptual loss, to the case $N_{\rm NNN} = 0$. The description becomes particularly simple for $N_{\rm cl} = 1$, since the states can be labeled simply by $b = 2p-1$, with p the position of the "center of mass" of the clusters:

$$|\uparrow\downarrow\downarrow\ldots\rangle \equiv |1\rangle \tag{S12}$$

$$|\uparrow\uparrow\downarrow\downarrow\ldots\rangle \equiv |2\frac{3}{2} - 1\rangle = |2\rangle \tag{S13}$$

$$|\downarrow\uparrow\downarrow\downarrow\ldots\rangle \equiv |3\rangle \tag{S14}$$

$$\ldots \tag{S15}$$

The advantage of this labeling is that the states are now sequentially connected by the Hamiltonian, i.e., $\langle b| H |b'\rangle \neq 0 \Leftrightarrow (b-b') = 0, \pm 1$ and thus naturally define a chain. Subtracting the additive constant Δ, one then finds again equation (2) of the main text, i.e.,

$$H_{\rm A} = \frac{\Omega}{2} \sum_{b=1}^{2L-2} \Big[|b\rangle \langle b+1| + |b+1\rangle \langle b| + h_b |b\rangle \langle b| \Big], \tag{S16}$$

where

$$h_b = \begin{cases} 0 & (\text{if } b \text{ odd}) \\ 2\delta V_{b/2}/\Omega & (\text{if } b \text{ even}). \end{cases} \tag{S17}$$

B. Non-reducibility to a free problem in dual space

We comment here on the fact that it is crucial to adopt the Fock-space description in order to reduce the problem to an Anderson one. In principle, accounting for the cluster-preserving property discussed above and in the main text, one could imagine to recast the problem in terms of diffusing domain walls (i.e., local configurations like $\uparrow\downarrow$ and $\downarrow\uparrow$) on the chain. In the case of open boundary conditions we are interested in, this could be intuitively pictured as follows: for later convenience, let us add two factitious (up) spins at the edges of the chain; for example, an $L=3$ configuration like $|\downarrow\downarrow\uparrow\rangle$ reads now $|(\uparrow)\downarrow\downarrow\uparrow(\uparrow)\rangle$, where the new additions are denoted within brackets. Now, let us define a model on the bonds between sites, instead of on the sites themselves; we now define domain walls as particles $|\uparrow\downarrow\rangle \to |1\rangle$, $|\downarrow\uparrow\rangle \to |1\rangle$ and intra-cluster bonds as holes $|\uparrow\uparrow\rangle \to |0\rangle$, $|\downarrow\downarrow\rangle \to |0\rangle$, such that the configuration in the example above becomes $|(\uparrow)\downarrow\downarrow\uparrow(\uparrow)\rangle \to |1010\rangle$. Although it may look like a two-to-one mapping, having fixed the boundaries to be up spins actually makes the mapping bijective between the space of all possible $(L+2)$-spin configurations with fixed boundaries (space dimension 2^L) and all the possible configurations of $L+1$ bonds with an *even* number of particles, since domain walls always come in pairs (space dimension 2^L). If this were a system of diffusing free particles, then hopping from one site to the next or previous one would always yield the same change in energy regardless of the configuration of the remaining particles. However, it is easy to find a counterexample: the process $|1010\rangle \to |1100\rangle$

corresponds to $|\downarrow\downarrow\uparrow\rangle \to |\downarrow\uparrow\uparrow\rangle$ and yields an energy shift $+\delta V_2$. On the other hand, $|0011\rangle \to |0101\rangle$ corresponds to $|\uparrow\uparrow\downarrow\rangle \to |\uparrow\downarrow\uparrow\rangle$ and yields instead $-\delta V_2$. The sign of the energy difference between a given configuration and the new configuration, where a particle has been moved to an adjacent site depends on the parity of the number of particles preceding the discplaced particle: in the spin language, it corresponds to determining whether the domain wall that is being moved is a left domain wall $\downarrow\uparrow$ — in which case, moving it left increases the number of actual interacting excitations, while moving it right decreases it — or a right one $\uparrow\downarrow$ — in which case the situation is reversed. Hence, these "particles" must interact via a non-trivial and non-local term. Even if we distinguish between left and right domain walls, i.e., by mapping $|\downarrow\uparrow\rangle \to |L\rangle$ and $|\uparrow\downarrow\rangle \to |R\rangle$ we do not obtain a free diffusive problem: in fact, in this case the parity is not a problem any more, but particles of type L and R experience a mutual hard-core repulsion, which is necessary to avoid excluded processes such as annihilation of excitation clusters. Another way of seeing this is that the only physical configurations in this space are the ones where the first particle must be R and the last one L and each R can only be followed (and preceded) by an L and vice versa. Therefore, to avoid a physical configuration evolving into a non-physical one, it must be impossible for L and R particles to overcome each other. In spite of the interaction taking a much simpler form, the problem still does not reduce to free diffusion.

V. DETAILS OF THE NUMERICAL SIMULATIONS AND COMPARISON WITH THE EXPERIMENTAL DATA

A. Two-atom case

In order to account for possible incoherent evolution of the excitations, we model the two-atom system using a master equation of the form

$$\dot{\rho} = i[\rho, H] + \mathcal{L}_{\text{loss}}(\rho) + \mathcal{L}_{\text{deph}}(\rho), \tag{S18}$$

where H is the Hamiltonian (1) and

$$\mathcal{L}_{\text{loss}}(\rho) = \frac{\gamma_{\text{loss}}}{2}\left(\sum_i 2\sigma^-_{\uparrow a,i}\rho\sigma^+_{\uparrow a,i} - \left\{\sigma^+_{\uparrow a,i}\sigma^-_{\uparrow a,i}, \rho\right\}\right) \tag{S19a}$$

$$\mathcal{L}_{\text{deph}}(\rho) = \frac{\gamma_{\text{deph}}}{2}\left(\sum_i \sigma^z_{\uparrow\downarrow,i}\rho\sigma^z_{\uparrow\downarrow,i} - \rho\right) \tag{S19b}$$

are the phenomenological Lindblad superoperators accounting for atom loss if the atom is excited in the Rydberg state and pure dephasing of the $|\downarrow\rangle - |\uparrow\rangle$ transition with rates γ_{loss} and γ_{deph} respectively. Here we model the loss by introducing an auxiliary level $|a\rangle$ and $\sigma_{\alpha\beta,i}$ are the usual Pauli matrices in the basis of $|\alpha\rangle, |\beta\rangle$ states acting on i-th atom. When we consider atom loss, the population in the auxiliary state is interpreted as the population in the Rydberg state, namely

$$P^{\text{eff}}_{\uparrow\uparrow} = P_{\uparrow\uparrow} + P_{\uparrow a} + P_{a\uparrow} + P_{aa} \tag{S20a}$$

$$P^{\text{eff}}_{\uparrow\downarrow} = P_{\uparrow\downarrow} + P_{a\downarrow} \tag{S20b}$$

$$P^{\text{eff}}_{\downarrow\uparrow} = P_{\downarrow\uparrow} + P_{\downarrow a}. \tag{S20c}$$

In order to account for the imperfect state preparation we consider the initial two-atom state in the $\{|\uparrow\uparrow\rangle, |\uparrow\downarrow\rangle, |\downarrow\uparrow\rangle, |\downarrow\downarrow\rangle\}$ basis to be of the form

$$\rho(0) = \begin{pmatrix} P_{\uparrow\uparrow} & 0 & \eta_1\sqrt{P_{\downarrow\uparrow}}\sqrt{P_{\uparrow\uparrow}} & 0 \\ 0 & P_{\uparrow\downarrow} & 0 & \eta_1\sqrt{P_{\downarrow\downarrow}}\sqrt{P_{\uparrow\downarrow}} \\ \eta_1\sqrt{P_{\downarrow\uparrow}}\sqrt{P_{\uparrow\uparrow}} & 0 & P_{\downarrow\uparrow} & 0 \\ 0 & \eta_1\sqrt{P_{\downarrow\downarrow}}\sqrt{P_{\uparrow\downarrow}} & 0 & P_{\downarrow\downarrow} \end{pmatrix}. \tag{S21}$$

This particular form of the initial density matrix is motivated by the fact that only its diagonal parts - the probabilities $P_{\uparrow\uparrow}, P_{\uparrow\downarrow}, P_{\downarrow\uparrow}, P_{\downarrow\downarrow}$ - were measured in the experiment. In (S21) η_1 parametrizes the initial coherence of the first atom and we take the coherence between the states of the second atom to be zero.

We solve the master equation (S18) numerically for $\eta_1 \in \{0, 0.25, 0.5, 0.75, 1\}$ and a range of values of $\gamma_{\rm loss}$ and $\gamma_{\rm deph}$. We then seek the parameters which minimize the squares of the difference between experimental and simulated data $\chi^2 = \sum_{\alpha,\beta\in\{\uparrow,\downarrow\}} \sigma^2_{\alpha\beta}$, where

$$\sigma^2_{\alpha\beta} = \frac{\sum_i \left(P_{\alpha\beta}(t_i) - P^{\rm sim}_{\alpha\beta}(t_i)\right)^2}{N}, \tag{S22}$$

where N is the number of data points (times t_i when the measurements were taken) and $P^{\rm sim}$ are the probabilities obtained by solving the Eq. (S18). Using the experimental initial values $(P_{\uparrow\uparrow}, P_{\uparrow\downarrow}, P_{\downarrow\uparrow}, P_{\downarrow\downarrow}) = (0.2, 0.63, 0.04, 0.13)$ for $\Delta = 0$ and $(0.13, 0.64, 0.04, 0.19)$ for $\Delta = -V_{\rm NN}$, we find the best results for $\eta_1 = 0.75$ and $(\gamma_{\rm loss}, \gamma_{\rm deph}) = (0, 0.5)\ \mu{\rm s}^{-1}$ which are used in Fig. 1.

Furthermore, we have verified that including the motion of the atoms in the traps has a negligible effect on the simulated dynamics which is consistent with $\gamma_{\rm loss} = 0\ \mu{\rm s}^{-1}$. This was done by considering the atoms to have velocities drawn from the normal distributions $p(v^i_k) \propto \exp(-\ {v^i_k}^2/2\sigma_v^2)$, where $\sigma_v = \sqrt{k_B T/m}$, $i = 1, 2, 3$ denotes the Cartesian coordinate and k labels the position of the atom. This leads to the time dependent interaction term in the Hamiltonian by replacing

$$\delta\mathbf{r}_{k+l} - \delta\mathbf{r}_k \to \delta\mathbf{r}_{k+l} - \delta\mathbf{r}_k + (\mathbf{v}_{k+l} - \mathbf{v}_k)t. \tag{S23}$$

The errors for the data plotted in Fig. 1 are taken to be the statistical mean errors $\epsilon_{\alpha\beta} = \sqrt{P_{\alpha\beta}(1 - P_{\alpha\beta})/N_{\rm meas}}$, where $\alpha, \beta \in \{\uparrow, \downarrow\}$ and $N_{\rm meas}$ is the total number of measurements (i.e. $P_{\alpha\beta} = N_{\alpha\beta}/N_{\rm meas}$ for each time and $N_{\alpha\beta}$ is the number of times when the first atom was measured to be in state α and the second in state β). In all cases the displayed finite size of the data points is equal or larger than the statistical errors.

In Fig. S2 we display the effects of changing the parameters driving the main sources of decoherence in our simulations. In all panels the first column shows oscillations driven via the ground state $|\downarrow\downarrow\rangle$ ($\Delta = 0$ in (S7)), while the second displays the case of driving them through the doubly-excited state $|\uparrow\uparrow\rangle$ ($\Delta = -V_{\rm NN}$ in (S7)).

In panel (a) we increase the dephasing rate from the optimized value $\gamma^{\rm fit}_{\rm deph} = 0.5\ \mu{\rm s}^{-1}$ while keeping all the other parameters fixed. We notice that this – consistently with the naive expectation – dampens the oscillations in both columns.

In panel (b) we multiply the experimental trap widths σ_α by a factor f, so that the new widths are isotropically rescaled,

$$\sigma_\alpha \to \tilde{\sigma}_\alpha = f\sigma_\alpha, \quad (\alpha = 1, 2, 3). \tag{S24}$$

We see that, as the positional disorder is consequently increased, the first column remains largely unaffected, while the second one shows higher and higher dampening of the oscillations. This confirms the relevance of this kind of disorder when relying on the facilitation mechanism. We note the better agreement between the simulations and the data for $f = 1.5$, $f = 2$. This potentially indicates an underestimation in the spread of the atomic positions. The σ_α's are inferred from the tweezers' waists and from the atomic temperatures (assuming thermal equilibrium of the atoms in the trapping potential). We believe that the observed discrepancy may originate from slight (trap-dependent) deviations of the light intensity distribution of the tweezers from perfect Gaussians with all the same waists and longitudinal positions. Although the conclusions of the present paper are not strongly affected by this mismatch, further investigation of this point will be the subject of future experimental work.

In panel (c) we focus instead on the temperature within the scheme described above. Here, we model the effect of the non-zero temperature by making the interatomic distance time dependent according to (S23). We display the values both below and above the experimental estimate $T^{\rm exp} \approx 50\ \mu{\rm K}$.

Another source of decoherence is the effect of the interaction on the atomic motion. In order to provide a rough estimate of its influence we consider the classical equations of motion of a system of two atoms which interact via a van-der-Waals potential $V(r)$. Setting $t = 2\ \mu{\rm s}$ to be the duration of an experimental run, we find for the relative atomic displacement due to the interaction $\approx 0.035\ \mu{\rm m}$ for the two-atom case parameters and $\approx 0.11\ \mu{\rm m}$ for the eight-atom case ones. Recalling the width of the traps $\sigma \leq 0.12\ \mu{\rm m}$, we see that even if the atoms were not trapped they would not have enough time to move away beyond the width of the traps. Furthermore, the same order of displacements is obtained on average in the lowermost row of Fig. S2(c) and does not yield any improvement in the agreement between numerics and experimental data, possibly signaling that this effect is in reality much smaller and therefore negligible compared to other sources of decoherence on the timescales of the experiment.

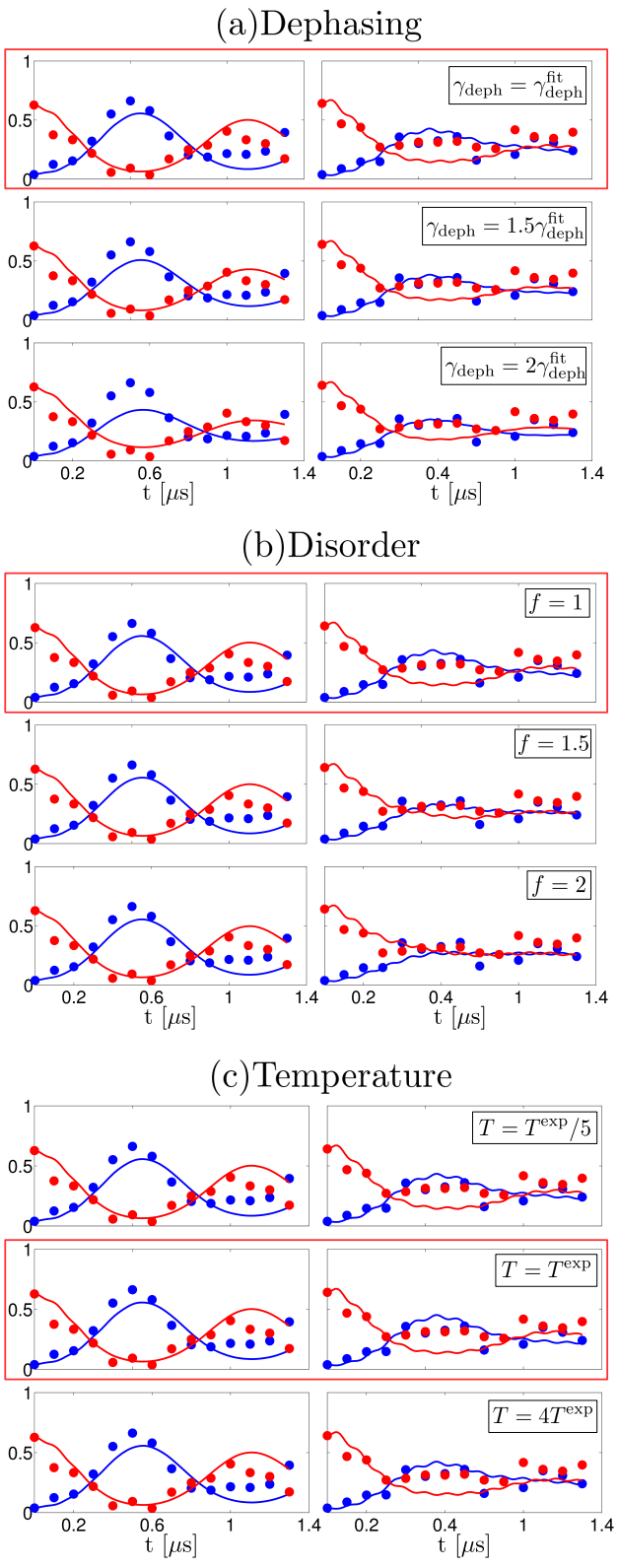

FIG. S2. Impact of different decoherence sources. All panels show the time evolution of the probabilities $P_{\uparrow\downarrow}$ (blue) and $P_{\downarrow\uparrow}$ (red). The left (right) column corresponds to driving through the $|\downarrow\downarrow\rangle$ state, $\Delta = 0$ ($|\uparrow\uparrow\rangle$ state, $\Delta = -V_{\rm NN}$). The circles represent the experimental data reported in Fig. 1 of the main text. The solid lines are the numerical simulations of (S18) using the optimal values $\gamma_{\rm loss} = 0$ and $\eta_1 = 0.75$. Panel (a) shows a sequence for increasing dephasing rate $\gamma_{\rm deph}$. Panel (b) corresponds to varying the amplitude of the positional noise of the atoms and in panel (c) we account for the thermal motion of the atoms (see text for details). Here $\gamma^{\rm fit}_{\rm deph} = 0.5\ \mu{\rm s}^{-1}$, $\sigma_1 = 1\ \mu$m, $\sigma_2 = \sigma_3 = 120$ nm and $T^{\rm exp} = 50\ \mu$K. All the simulations shown were obtained by averaging over 200 realizations of the disorder. The red boxes in (a),(b),(c) highlight the cases corresponding to the experimental parameters.

B. Eight-atom case

Importantly, in the two-atom case, we have observed that the inclusion of the loss or dephasing mechanisms has relatively small quantitative effect (for the relevant values of the parameters γ_{loss} and γ_{deph}) on the simulated excitation dynamics, so that neglecting those effects still yields a good agreement with the data.

Based on this observation and seeking a qualitative understanding of the dynamics in the eight-atom chain, we simulate the results presented in Fig. 4(b-e) by exactly evolving the initial density matrix with the time-evolution operator $U(t) = \exp(-iHt)$, where H is given by the Eq. (S7), (S11) for the full and effective model respectively. We assume the initial state to be a pure state constructed from the experimental data (excitation probabilities) in the same way as in (S21).

In Fig. S3 we provide an additional comparison between the spreading of the excitations along the chain in the experimental and numerical data. To this end, we define an effective spatial distribution of the excitations as

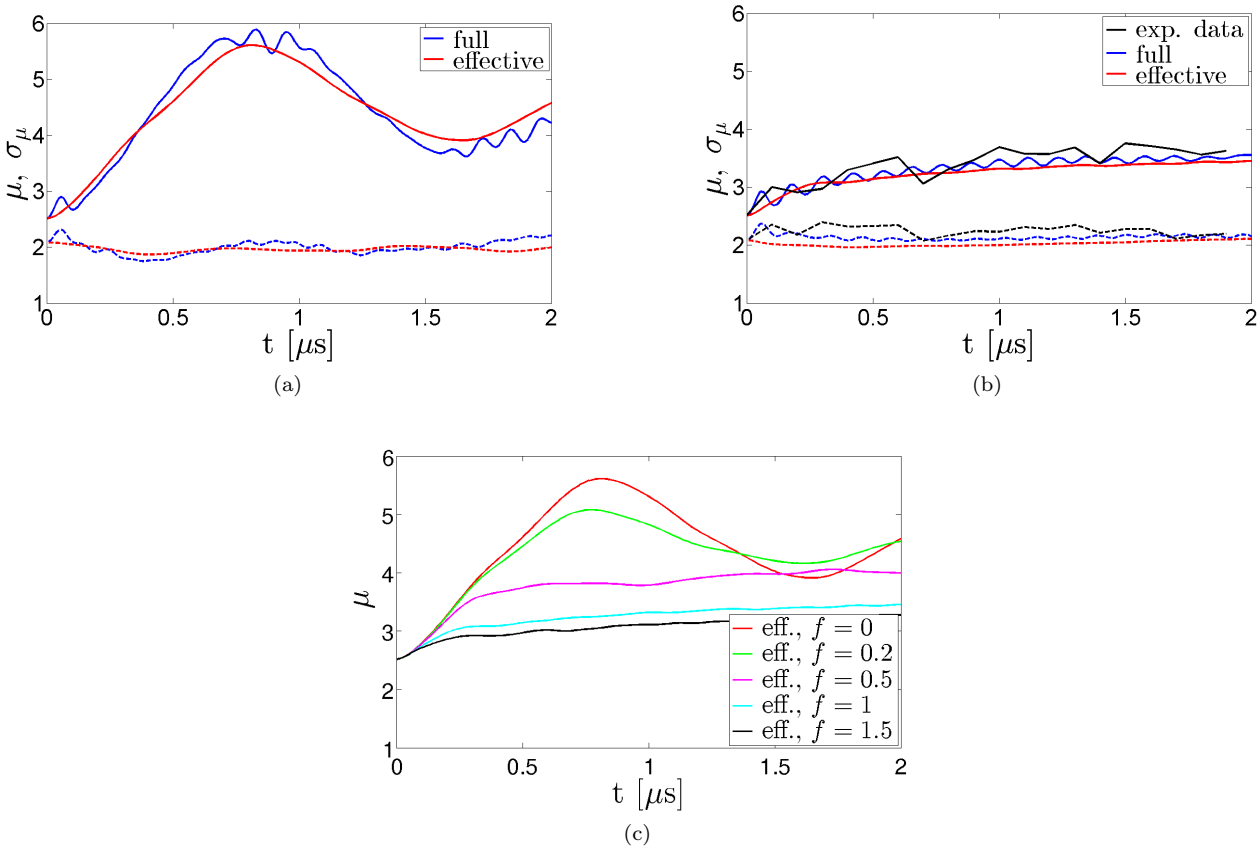

FIG. S3. (a,b) Mean μ (solid lines) and variance σ_μ (dashed lines) as functions of time for the same dataset used for Fig. 4. Panel (a) here corresponds to the ideal (no disorder) case, (i.e. panels (c,e) in Fig. 4). Panel (b) corresponds instead to the case accounting for positional disorder (panels (a,b,d) in Fig. 4). Here, panel (b) shows that the global properties of the position distribution are well reproduced for both the effective and full numerical models. As expected, the comparison with panel (a) highlights the difference in behavior due to the presence of disorder. (c) Effect of different disorder strengths on the mean μ. The disorder is varied by rescaling the trap widths by f according to Eq. (S24). As one would intuitively expect, the curves interpolate between the two limiting cases $f = 0$ and $f = 1.5$. For the chosen initial condition, the system becomes localized around $f \lesssim 0.5$.

$$p_k = \frac{\langle n_k \rangle}{\sum_j \langle n_j \rangle} \tag{S25}$$

and we focus on its mean $\mu = \sum_k k p_k$ and variance $\sigma_\mu^2 = \sum_k (k-\mu)^2 p_k$. The results reported in Fig. S3 show good agreement for the low-order moments of the distribution between numerical and experimental data. In panel (c) we display the evolution of the mean μ under different disorder strengths, highlighting a qualitative change in behavior between $f = 0.2$ and $f = 0.5$, where f is the rescaling factor introduced in Eq. (S24).

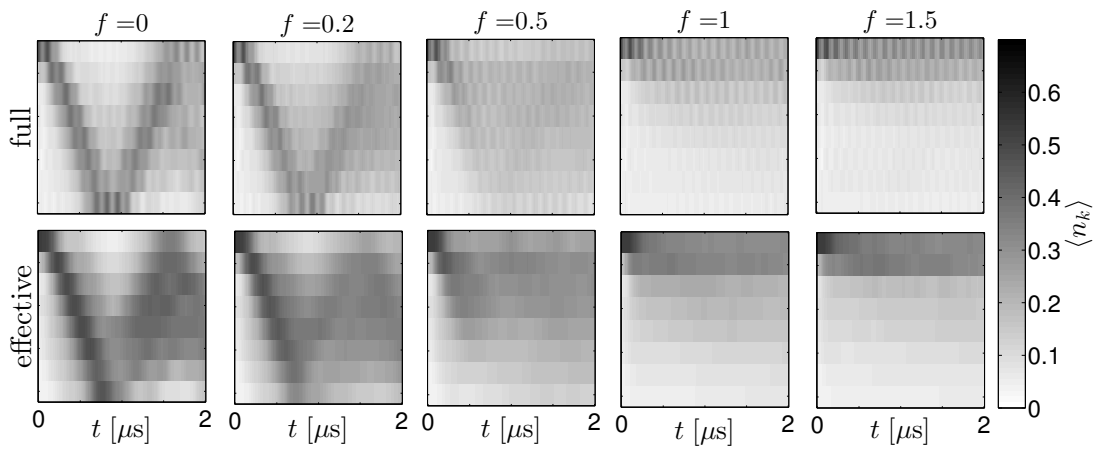

FIG. S4. Time evolution of site-resolved excitation probability obtained from numerical simulations of the full (topmost row) and effective (bottommost row) Anderson-Fock models for different disorder strengths. The initial conditions are the same as used in the main text and the disorder is averaged over 20 realizations for $f = 0.2, 0.5$, 50 for $f = 1.5$ and 100 for $f = 1$. The first column ($f = 0$) corresponds to panels (c) and (e) in Fig. 4 in the main text, the fourth one ($f = 1$) to (b) and (d). It is apparent that the localizing effects become more pronounced with increasing disorder strength.

Figure S4 qualitatively depicts the extent of the localization for different values of the disorder as a function of the trap rescaling factor f (Eq. (S24)). A quantitative characterization of the transport properties of this model is left for future investigation, but one can readily see that for the used initial conditions, the excitation propagation through the whole system is inhibited for disorder strengths above $f \lesssim 0.5$.